Stochastic analysis of a stadium roof from deterministic wind tunnel measurements

N. Blaise [a], V. Denoël [b]

[a,b]*Department of Architecture, Geology, Environment and Construction, University of Liège, Liège, Belgium,* [a]*N.Blaise@ulg.ac.be,* [b]*V.Denoel@ulg.ac.be*

1 INTRODUCTION

Dynamic analyses of structures under buffeting wind loads can be performed in a deterministic (Clough and Penzien, 1997) or stochastic (Preumont, 1994) context, both with a modal approach for computational efficiency reasons. In the first option, the forces are deterministically given, and the uncoupled modal equations of motion are solved either in the time domain with a step-by-step method, either in the frequency domain, with Fourier transformation. In the second option, the analysis relies on the determination of the Power Spectral Density (PSD) matrix of the structural response given that of the loading. The choice of one or another method usually depends on whether the loading is provided in the time or frequency domain and as a deterministic (a single time history) or stochastic manner.
From a designer's point of view, the wind loading can be defined using design codes (e.g. Eurocode, 2005) where analytical expressions of (i) the PSD of wind velocities (Davenport, Von Karman, etc) (ii) the coherence functions and (iii) the pressure coefficients are given to compute, finally, (iv) the PSD of the aerodynamic pressures. Design engineers are usually familiar with this probabilistic approach.

Alternatively, the design may be conducted from aerodynamic pressures measured in a wind tunnel. This approach is more realistic than the aforementioned codified procedure since a number of phenomena as (a) the aerodynamic instabilities, (b) aerodynamic admittance (Scanlan and Jones, 1999), (c) site effects are taken into account. Pressures are thus given as unique (deterministic) time histories at each sensor. In a Finite Element context and a modal analysis, the generalized forces are computed from the measured pressures. With the firm wish to perform the analysis in a stochastic manner (for a number of good reasons mentioned next), we suggest to fit a probabilistic model to the measured data. Such a model could be fitted to the measured pressures right away, or any other subsequent quantity such as the generalized forces.

The following discussion is about the most favorable quantity that has to be fitted and how to do it appropriately in view of typical measurement imperfections.

2 STUDIED STRUCTURE : "LE GRAND STADE DE LILLE METROPOLE"

The considered structure is the roof of the stadium "Le Grand Stade de Lille Métropole" currently under construction at Lille, France. It is composed of an upper envelope supported by its structural frame. A part of this roof is retractable in order to close the stadium during exhibitions or severe climatic conditions. Its specificities are a retractable roof and a moving half-grass. Its dimensions are 230x200x36 meters. As depicted in Figure 1, the roof is made up of three parts: above the ambulatories, above the terraces and above the playground. The frequency of the first mode is equal to 0.475 Hz and the first eleven modes have a natural frequency lower than 1 Hertz. The first twenty-one modes are kept for the modal analysis which corresponds to the frequency range [0; 1.415] Hz.

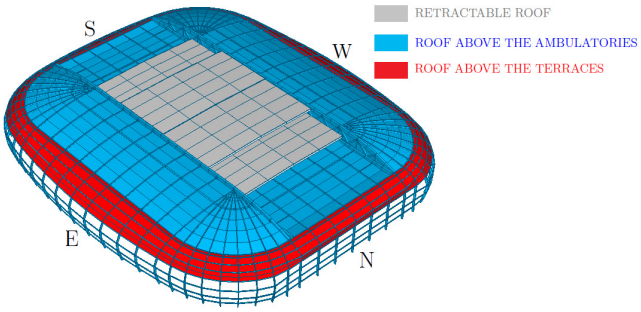

Figure 1. Different parts of the roof.

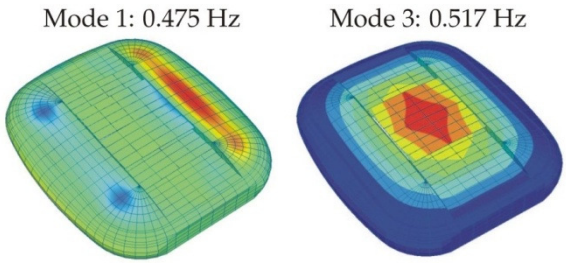

Figure 2. Modal vertical displacements and associated frequencies.

Figure 2 depicts the first and third modes. The first one is longitudinal antisymmetric vertical and the third mode represents a general vertical movement of the retractable roof. A modal damping (ξ) equals to 1% for each mode is considered.

3 WIND TUNNEL SIMULATION

3.1 *Simulated wind properties*

The wind is simulated in the wind tunnel to target wind properties of Eurocode, 2005. A IIIa terrain category is appropriate to represent the surrounding of the stadium. Table 1 presents the main parameters of this characterization. The loads induced by these wind properties correspond to the Service Limit State ones.

Table 1. Target wind properties.

Mean wind Reference velocity pressure	$V_m(z_s)$=28.3 m/s $q_{mean}(z_s)$=491.7 N/m²	Turbulence Intensity Peak velocity pressure	$I_v(z_s)$=19 % $q_p(z_s)$=1133 N/m²

3.2 *Pressures acquisition*

Wind tunnel measurements have been carried out at the "Centre Scientifique et Technique du Bâtiment" at Nantes in France. Figure 3 shows the 1/200 scaled model in the wind tunnel with the: (a) view of the exit turbine, (b) blocks to create the wind velocity, (c) and (d) surrounding buildings, (e) surrounding woods. Pressures at more than 500 sensors are simultaneously measured in the wind tunnel. The data acquisition is limited by a sampling frequency which is equal to 2.92 Hz in full scale (200 Hz wind tunnel-scale); so the time step is equal to 0.342 seconds. Each measurement lasts about 105 minutes full scale. This paper considers only one configuration, 75° wind direction (see Fig. 4) and the retractable roof 100% closed. Twenty four wind directions have been tested for ten configurations of the retractable roof.

3.3 *Post processing of the acquired pressures*

It starts by separating the mean and the fluctuating part of the pressures; maps of the skewness coefficient and the positive and negative peak factors are also shown and explained, see Figure 5.

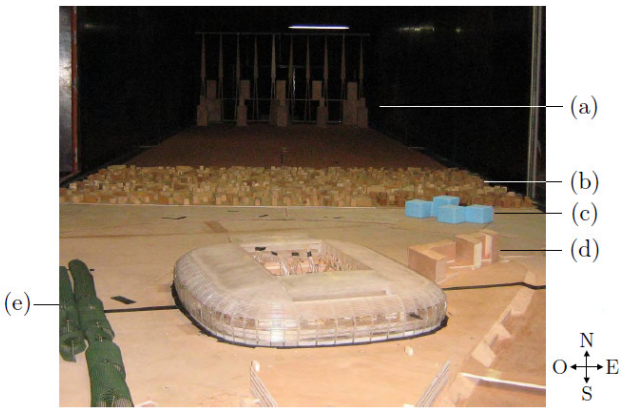

Figure 3. Scaled model of the stadium tested in the wind tunnel.

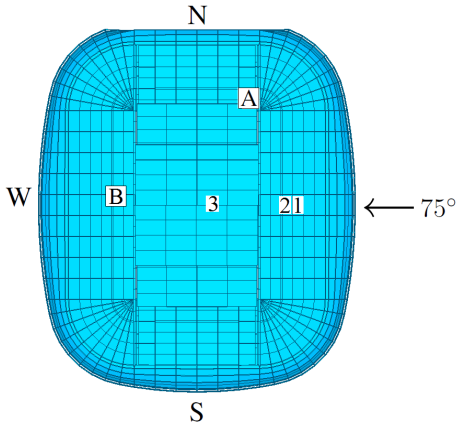

Figure 4. The studied direction of wind and location of some sensors used for further illustrations.

Further, PSD and coherence functions of the fluctuating part are computed, see Figures 6-7.
Wind pressures, $\mathbf{p}_{\mathrm{tot}}(t)$, can be separated:

$$\mathbf{p}_{\mathrm{tot}} = \boldsymbol{\mu}_{\mathrm{p}} + \mathbf{p} \quad (1)$$

where $\boldsymbol{\mu}_{\mathrm{p}}$ and $\mathbf{p}(t)$ are respectively the mean and the fluctuation part of wind loads. As a first data post processing, maps of means and standard deviations of pressures can be computed and analyzed. Indeed, it offers a valuable understanding of the wind flow around the structure. These maps are not disclosed in this paper because they show typical patterns, for example, in zones with sharp edges (Blaise, 2010).
Higher order statistics are also interesting statistical descriptors of the acquired pressures. They are typically interesting when it comes to estimate extreme values, i.e. those related to small occurrence probabilities. The analysis of the skewness coefficient map indicates the zones on the roof where the wind flow is typically non-Gaussian and requires a dedicated attention for the determination of extreme forces (Beirlant et al., 2004; Gupta and van Gelder, 2007). Alternatively, the importance of the extreme wind pressures may be appreciated by means of positive and negative peak factors, defined as:

$$\mathrm{g}^{(+)} = \frac{\mathrm{p_{max}} - \mu_{\mathrm{p}}}{\sigma_{\mathrm{p}}};\ \mathrm{g}^{(-)} = \frac{\mu_{\mathrm{p}} - \mathrm{p_{min}}}{\sigma_{\mathrm{p}}} \quad (2)$$

where $\mathrm{p_{max}}$, $\mathrm{p_{min}}$ are the minimum and maximum values of $\mathrm{p_{tot}}(t)$, respectively; σ_{p} is the standard deviation of the acquired pressures.

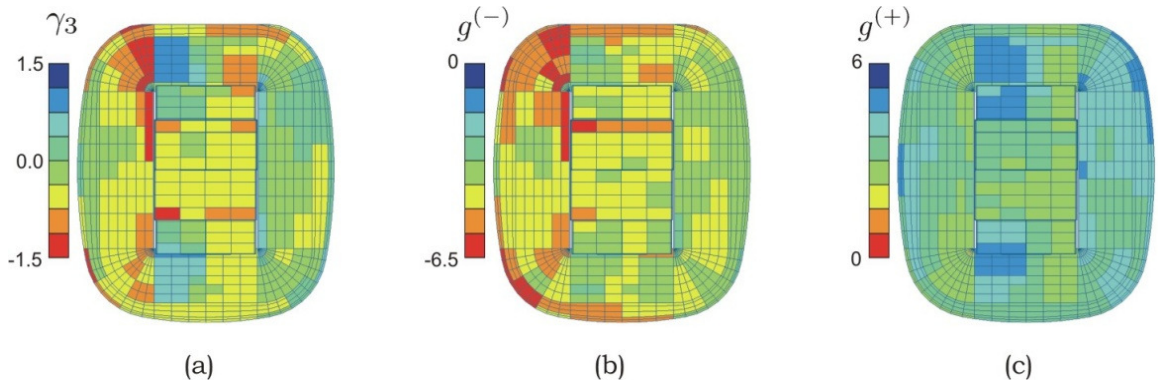

Figure 5. Maps of (a) the skewness coefficients of the pressure coefficients; (b) the negative peak factors; (c) the positive peak factors of the pressure coefficients.

These peak factors may in some cases drastically drift from the well-known range g ϵ [3.5; 4] as usually adopted for Gaussian processes. Figure 5-(a) depicts a skewness coefficient ranging from -1.5 to 1.5, which indicates a significant departure from symmetrically distributed variables in several parts of the structure. Figure 5-(b,c) evinces peak factors as large a 6~6.5, as well as an interesting similarity with the skewness coefficient map. In this case, positive skewness coefficients are associated to positive peak factors larger than the negative ones and vice versa.

Further, an interesting insight into the acquired data consists in analyzing the PSD of the measured pressures, see Figure 6. PSD's are computed using Welch's method with a Hamming window.

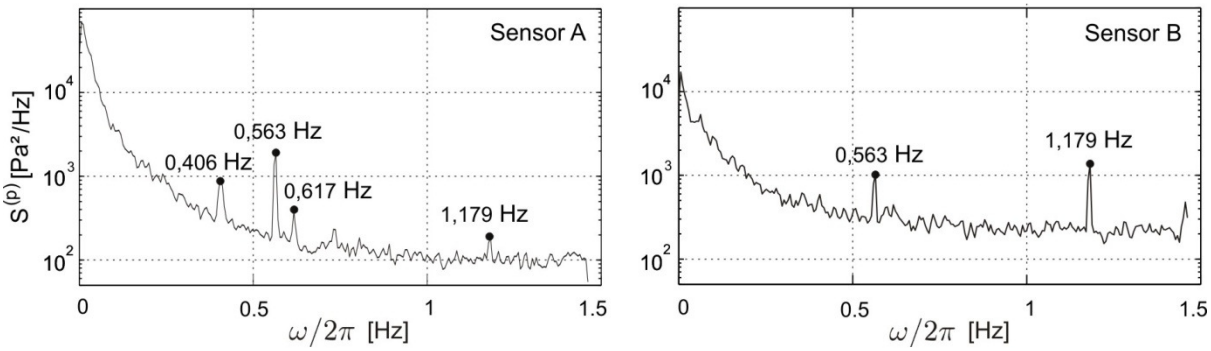

Figure 6. PSD of measured pressures at sensors A and B. The number of points is 512 in each window (total number of points is equal to 18432) with an overlap of 50%.

This operation reveals a typical decreasing PSD. Besides, it appears that almost all acquired pressures are noised by significant harmonic oscillations (they are pointed with labels and dots in Figure 6). Several reasons are possible to explain these spurious harmonic frequencies: rotation speed of turbine blades, flexibility of the scale model, flexibility of the turning table, etc. These noise frequencies are undesired and have a possible important influence on the structural design and thus must be filtered out. Beyond approximately the two-third of the Nyquist frequency, the PSD seems to be constant due to possible limitations in the acquisition system.

Figure 7 shows the real and imaginary parts of the coherence functions pairing sensor 1 to sensors 2, and 3, located in the alongwind direction. Although standards usually neglect the imaginary part of the coherence and model the real part as a decreasing exponential (at least concerning the wind velocity) (Dyrbye and Hansen, 1997), we may observe that this model (adopted from free field turbulence) is far from reality. The global decrease of the real part rather indicates first a short plateau, then a rapid decrease, followed by a somewhat significant noise. The imaginary part is of the same order of magnitude as the real part. Notice Figure 7 indicates, for both the real and imaginary parts, more coherence between sensors 1 and 2, than 1 and 3 which is of course expected because of proximity.

Of paramount importance is the fact that the non-parametric estimates of the auto- and cross-PSD provide an erratic result, despite the periodogram averaging and window overlap. Actually an infinite set of pressures are in principle necessary to obtain a smooth non-parametric estimation of the PSD. This goes naturally beyond the physical limitations of any testing. As a matter of fact, the processing of a single recorded signal, as long as it may physically be, provides an erratic non-parametric estimate; and the new beginning of another experiment under the "same" conditions would yield a different PSD estimate. The discrepancy between both is as large as the signals are short. Furthermore, experience shows that the reproducibility of coherence functions is even worse.

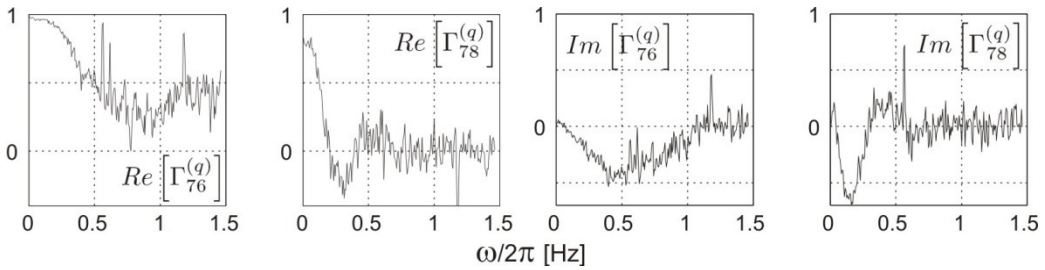

Figure 7**.** Real and imaginary parts of the coherence functions of pressures measures at sensors (1,2), (1,3).

4 DESIGN OF STRUCTURES FROM WIND TUNNEL MEASUREMENTS

The structure is analyzed next with various methods, but all of them are based on the modal superposition principle. Due to a diagonal damping matrix (see Sec. 2), the equations of motion are uncoupled and thus the dynamic computation is efficient in the modal basis; moreover the number of unknowns is also reduced. A common stage of these methods is the computation of the generalized forces, $\mathbf{p}^*(t)$, which is (deterministically) performed in the time domain, by projection of the fluctuation part of the measured pressures into the known modal space, characterized by mode shapes $\boldsymbol{\varphi}$. The equation of motion, in the modal basis, is solved with three different approaches:

1. Deterministic time domain (Det.−T.):

$$\mathbf{M}^*\ddot{\mathbf{q}} + \mathbf{C}^*\dot{\mathbf{q}} + \mathbf{K}^*\mathbf{q} = \mathbf{p}^* \tag{3}$$

where $\mathbf{M}^*$, $\mathbf{C}^*$ and $\mathbf{K}^*$ are respectively the generalized mass, damping and stiffness matrices (known from a FE model); $\mathbf{q}(t)$, $\dot{\mathbf{q}}(t)$ and $\ddot{\mathbf{q}}(t)$ are respectively the modal displacement, velocity and acceleration. Newmark's algorithm (Newmark and Rosenblueth, 1971) (constant acceleration) is used to solve (3).

2. Deterministic frequency domain (Det.−F.):

$$\mathbf{Q} = \mathbf{H}^*\mathbf{P}^* \tag{4}$$

where $\mathbf{Q}(\omega)$ is the Fourier transform of $\mathbf{q}(t)$; $\mathbf{H}^*(\omega)$ is the modal transfer function and $\mathbf{P}^*(\omega)$ is the Fourier transform of $\mathbf{p}^*(t)$. The inverse Fourier transform is then applied to $\mathbf{Q}(\omega)$ to obtain, if necessary, the time history $\mathbf{q}(t)$.

3. Stochastic frequency domain: (Stoch.)

$$\mathbf{S}^{(\mathrm{q})} = \mathbf{H}^*\mathbf{S}^{(\mathbf{p}^*)}\overline{\mathbf{H}^*}^{\mathrm{T}} \tag{5}$$

where $\mathbf{S}^{(\mathbf{p}^*)}(\omega)$ is the PSD matrix of the generalized forces and $\mathbf{S}^{(\mathrm{q})}(\omega)$ is the PSD matrix of the modal coordinates.

Thanks to their relative simplicity of implementation, analysis methods 1 and 2 are usually performed. The disadvantage of these analyses is that their results depend on unique measures which are not repeatable. On the contrary, analysis 3 precisely presents the advantage of depending on a probabilistic property fitted on the measured data (so not strongly dependent on a non repeatable measurement).

5 FITTING OF A MODEL ONTO THE GENERALIZED FORCES

Section 3 has thrown light onto some shortcomings related to the measured signals. To handle noise frequencies, in a deterministic method, is not an easy task. So if such an analysis is applied, we suggest checking at least that noise frequencies are not coincident with the structural natural frequencies. A proposed criterion is to fix a range around each natural frequency where no noise frequencies are to be present.

The range could be the peak width of the transfer function at half-height. In that case, the following condition has to be check for every noise frequencies:

$$f_{noise} \notin [(1-\xi)f_n;\ (1+\xi)f_{nat}] \quad (6)$$

where f_{noise} , ξ and f_n are the noise frequency, damping ratio and natural frequency, respectively. For this study, this criterion has been checked and validated as shown in Figure 8.

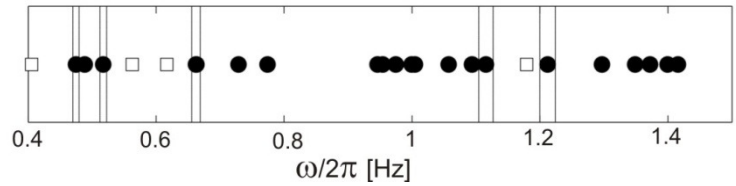

Figure 8. Assessment of the proposed criterion. The empty squares are the four noise frequencies, full circle are the natural frequencies and the vertical lines are the conditions in eq. (6).

On the contrary, the stochastic model is a smart way to bypass the drawbacks related to these noise frequencies. The fitting can be done at different levels of the stochastic analysis, e.g. to the acquired pressures. Nevertheless to fit a probabilistic model directly to the generalized forces is more attractive because (i) the number of auto-PSD's to fit is reduced to the number of modes shapes, (ii) the number of coherence function between generalized forces may be limited to the modes with clustered natural frequencies (Denoël, 2009). A comparative study (not reported here for conciseness) has shown that this solution is optimum (Blaise and Denoël, 2011).

Thus, we fit a stochastic model onto the deterministic generalized forces, $\mathbf{S}^{(\mathbf{p}^*)}(\omega)$, for the whole frequency range, that thus does not take into account the noise frequencies. The proposed solution is to i) calculate the PSD using a non parametric method ii) identify the noise frequencies iii) filter the noise frequencies by a band stop iv) perform a parametric estimate onto the filtered generalized forces.

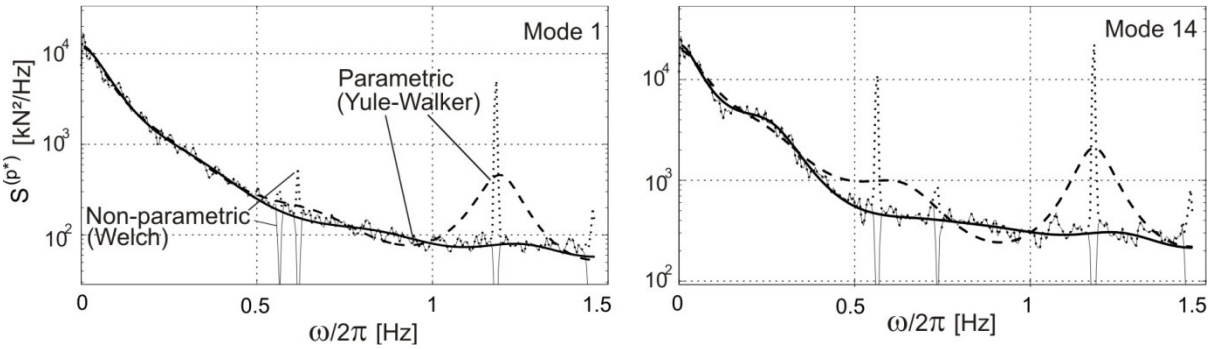

Figure 9. Fitting of a probabilistic model to the generalized force in mode 1 and 14. Non parametric or parametric estimates, before and after bandstop filtering.

The fitting to generalized forces is illustrated in Figure 9 for the 1th and the 14th mode, which are significantly affected by spurious harmonics. The solid and dotted lines represent the non-parametric PSD estimates of the raw generalized forces and of the filtered generalized forces around the noise frequencies, respectively. Thick lines represent the parametric model, a 10th-order Yule-Walker model, obtained from the raw and filtered generalized forces, respectively. One may observe that the successive application of a bandstop filtering and parametric estimation provides a smooth acceptable PSD. Moreover it shows that the raw application of the parametric

estimate onto the noise generalized forces is not recommended. Indeed it leads to under- and overestimations of the PSD.

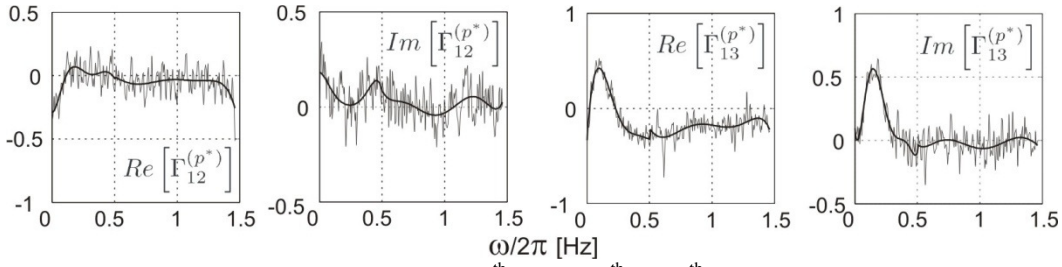

Figure 10. Coherence functions between the 1th and the 2th and 3th generalized forces.

The real and imaginary parts of the coherence functions between generalized forces in modes (1,2) and (1,3) are represented in Figure 10. They are fitted using polynomial functions of 6th to 8th order to two ranges of frequency [0; $1/3f_{Ny}$] Hz and [$1/3f_{Ny}$; f_{Ny}] Hz where f_{Ny} is the Nyquist frequency.

On top of providing a simple way to treat these noise frequencies it also provides a model that is consistent with physical intuition and offers smoothness and robustness against spurious harmonics and repeatability. Also the fitting onto the generalized forces instead of the measured pressures simplifies the procedure because the number of fitting is reduced due to the modal truncation.

6 RESULTS

6.1 *Modal coordinates*

As a first comparison, the PSD of modal coordinates obtained with the three analysis methods are given in Figure 11.

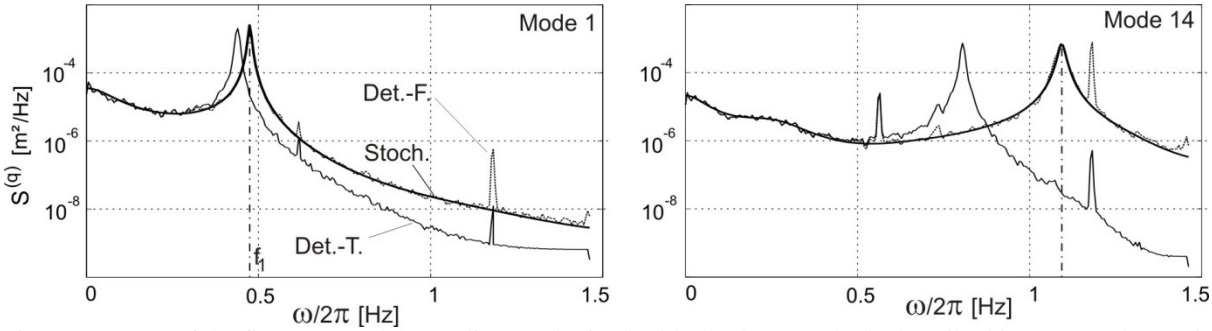

Figure 11. PSD of the first two modal coordinates obtained with the three methods described in Sec. 2. The vertical dash-dotted line indicates the natural frequency.

Resonant peaks of curves Det.-F. and Stoch. are precisely on the natural frequency whereas the peak associated to the curve Det.-T. appears before the natural frequency. This frequency stretch is a well known shortcoming of time stepping methods (Gmür, 2008), resulting from a large time step compared to the natural period (one sixth for the first mode in this case study). Curves Det.-F. and Stoch. are virtually superimposed and results obtained are similar in terms of standard dev-

iations. Of more importance, the curve Stoch. proves to be superior since: (i) it provides a smooth result that will therefore ensure a reliable estimate of the PSD; (ii) noise frequencies are totally pruned (see the remaining noise frequency at 1.179 Hz).

7 CONCLUSIONS

In conclusion, the use of a stochastic approach from deterministic wind tunnel measurements is benchmarked against a deterministic approach. The main argument is obviously the flexibility in pre-processing the time histories measured in the wind tunnel in order to smoothen them. It also allows a model consistent with physical intuition. This study also reveals the necessity of third order stochastic analysis (Denoël and Degée, 2006; Gusella and Materazzi, 1998) to take into account the non Gaussianity of the applied pressures. Thus, current researches are focused on the extension of the probabilistic model fitting to bispectrum of the generalized forces.

8 ACKNOWLEDGEMENTS

We would like to acknowledge the “Centre Scientifique et Technique du Bâtiment” in Nantes in France and also the design office “Greisch” in Liège, in Belgium for having provided the measurements in wind tunnels which was the matter of this work.

9 REFERENCES

Beirlant, J., Goegebeur, Y., Teugels, J., Segers, J., Waal, D. D. & Ferro, C., 2004. Statistics of Extremes, theory and applications, Wiley, Chichester, England.

Blaise, N., 2010. Etude du comportement d’une toiture de grandes dimensions soumise à un vent turbulent. Application: le Grand Stade de Lille Métropole. Travail présenté en vue de l’obtention du grade d’Ingénieur civil construction à finalité approfondie, Faculté des Sciences Appliquées, Université de Liège.

Blaise, N., Denoël, V., 2011. Optimal processing of wind tunnel measurements in view of stochastic structural de sign of large flexible structures. Wind Tunnel, inTech Edition. In press.

Clough, R. W., Penzien, J., 1997. Dynamics of structures. Mc Graw-Hill: Civil Engineering series (second edition).

Davenport, A. G., 1961. The application of statistical concepts to the wind loading of structures, Proceedings of the Institute of Civil Engineers 19, 449–472.

Denoël, V., Degée, H., 2006. Non Gaussian Response of Bridges Subjected to Turbulent Wind Effect of the non Linearity of Aerodynamic Coefficients, ECCM06, 3rd European Conference on Computational Solid and Structural Mechanics, Lisbon, Portugal.

Denoël, V., 2009. Estimation of modal correlation coefficients from background and resonant responses. Structural Engineering And Mechanics 32(6): 725-740.

Dyrbye, C., Hansen, S. O., 1997. Wind loads on structures. John Wiley & Sons.

Eurocode, 2005. Actions sur les structures – Partie 1-4 : Actions générales –Actions du vent. Comité Européen de normalisation, Réf. n° EN 1991-1-4 : 2005 F.

Gmür, T., 2008. Dynamique des structures. Analyse modale numérique. Presses polytechniques et universitaires romandes.

Gupta, S., van Gelder, P., 2007. Extreme value distributions for nonlinear transformations of vector gaussian processes. Probabilistic Engineering Mechanics 22(2): 136–149.

Gusella, V., Materazzi, A. L., 1998. Non-Gaussian response of MDOF wind exposed structures: Analysis by bicorre lation function and bispectrum. Meccanica, 33-3, 299-307.

Holmes, J. D., 2007. Wind Loading on Structures, 2nd edition edn, SponPress, London.

Newmark, N.M., Rosenblueth, E., 1971. Fundamentals of Earthquake Engineering (Civil engineering and engineer ing mechanics series). Prentice-Hall in Englewood Cliffs, N.J.

Preumont, A., 1994. Random Vibration and Spectral Analysis. Ed. K.A. Publishers. Kluwer Academic Publishers.

Scanlan, R. H., Jones, N. P., 1999. A form of aerodynamic admittance for use in bridge aeroelastic analysis. Journal Of Fluids And Structures 13(7-8): 1017-1027.